Publications of the Astronomical Society of the Pacific
109: 614–627, 1997 May

Night-Sky High-Resolution Spectral Atlas of OH Emission Lines for Echelle Spectrograph Wavelength Calibration. II.[1,2]

DONALD E. OSTERBROCK AND JON P. FULBRIGHT

University of California Observatories/Lick Observatory, Board of Studies in Astronomy and Astrophysics, University of California, Santa Cruz, California 95064
Electronic mail: don@ucolick.org, jfulb@ucolick.org

THOMAS A. BIDA

W. M. Keck Observatory, California Association for Research in Astronomy, Kamuela, Hawaii 96743
Electronic mail: tbida@keck.hawaii.edu

Received 1996 November 15; accepted 1997 January 20

ABSTRACT. The potential of night-sky emission lines recorded on every long-exposure astronomical spectrum, for wavelength calibration, is reemphasized. The previously published high-resolution atlas, based on spectra obtained with the Keck 10-m telescope on Mauna Kea and the HIRES high-resolution echelle spectrograph, is extended from 9000 to 10,600 Å, the present effective long-wavelength limit for reasonable exposure times with current CCDs. The extension of the atlas shows many OH night-sky lines, and makes it possible to identify them easily on high-resolution spectra. Accurate wavelengths and references to their sources are given. Measured intensity ratios for the resolved, well-measured lambda-type doublets are presented, and the probable errors in the listed wavelengths of the unresolved doublets, based on them, are discussed. Observations and identifications of a number of lines of weak satellite or intecombination bands of OH in the night-sky spectrum are discussed, and the "not proven" result of a search for OH lines in the $(10 - 5)$ and $(10 - 4)$ bands is mentioned.

1. INTRODUCTION

The numerous OH emission lines of the night-sky spectrum, although they contaminate every observed spectrum of a star, nebula, or galaxy, also provide a potentially useful wavelength-calibration spectrum taken automatically as a byproduct of that exposure. For high-resolution spectra, these OH lines are particularly appropriate because their laboratory wavelengths have been very accurately measured and published (Abrams et al. 1994), and because they are well distributed through the yellow, red, and infrared spectral regions. Thus at least a few of them appear in every order of high-resolution echelle spectrographs like the HIRES spectrograph on the Keck 10-m telescope (Vogt et al. 1994). To identify the OH lines on a spectrum an atlas in which the strongest lines are marked and hence instantly recognizable is very useful. Hence two of us, with several other collaborators, published such an atlas, based on then-available spectra, extending over the spectral range λλ5190– 8990 (Osterbrock et al. 1996, hereafter Paper I). In the present paper, based on more recently obtained spectra, we extend this atlas to λ10600, which is about the long-wavelength limit of currently available CCDs with reasonable exposure times.

[1]Lick Observatory Bulletin 1351.

[2]Based on observations obtained at the W. M. Keck Observatory, which is operated by the California Institute of Technology and the University of California.

2. OBSERVATIONAL DATA

The extension of the atlas to longer wavelengths contained in the present paper is based on two pairs of exposures of the night sky taken with HIRES by Bida, as listed in Table 1. "Left" and "right" are two different echelle settings, as explained in Paper I. The night-sky spectra were extracted from these exposures and were combined to provide complete spectral coverage from λ8795 to λ10600 (echelle orders 40 through 34) for this paper. Note that order 40 is included in Paper I and in this one, but with somewhat different central wavelengths, so that there are no gaps in the coverage between orders in either paper. In the present paper the resulting night-sky spectrum extends from λ8790 (in order 40) to λ10600 (in order 34). As in Paper I the slit widths were chosen to give a resolution ~ 0.2 Å at λ7000, while the dispersion at the CCD was 0.05 Å pix^{-1}, so the spectra were well sampled.

The wavelength scale was calibrated from the OH lines themselves, as described in Paper I, and the individual orders are plotted in Figs. 1 through 7. As in that paper the continuum was flattened and nearly entirely removed, and the intensity scale for each order was normalized so that its strongest line peaks at 1.00. Thus each order is plotted at a different intensity scale, and the noise level therefore differs from one order to the next. The noise also increases toward longer wavelength because of the decreasing sensitivity of the CCD. This atlas provides a good starting point for identifying night-sky lines in this spectral region which are likely to be recorded with currently available CCDs and exposure

TABLE 1
Journal of Night-Sky-Spectra Observations

	Shorter Wavelength		Longer Wavelength	
	left	right	left	right
Observer	Bida	Bida	Bida	Bida
Date	11 Jan 1996	10 Sep 1995	11 Jan 1996	11 Jan 1996
UT	5:52	10:18	6:14	6:30
Orders	36–47		30–36	
$\lambda\lambda$	7476–10035		9760–11990	
Exposure	25 min.	20 min.	15 min.	15 min.
α (1950)	00^h25^m	00^h52^m	00^h25^m	00^h25^m
δ (1950)	$+04°47'$	$+45°00'$	$+04°47'$	$+04°47'$
Zenith Distance (°)	39	33	44	48
Azimuth (°)	250	13	255	257

times comparable to those most observers on the Keck HIRES spectrograph use.

3. OH BANDS

All of the night-sky lines we identified in this spectral region are from the Meinel rotation-vibration bands of OH. Very accurate laboratory wavelengths for this band system have been measured and published by Abrams et al. (1994). Hence in the figures we label the OH lines by their designations in the standard spectroscopic notation used by these authors, and give the wavelength to 0.001 Å from their Table 29 (in which they are given to their full accuracy, 0.00001 Å). The standard spectroscopic notation, described by Herzberg (1950), is briefly summarized in the context of the OH Meinel bands in Paper I. As in that paper, the straight arithmetic mean of the wavelengths of the two components, e and f, is shown in the figures for all pairs in which the Λ-type doubling is smaller than 0.2 Å, about the effective limit of resolution for the Keck HIRES with the slit width commonly used, while the wavelengths of the individual components are shown for pairs with splitting larger than this limit. Furthermore, if two lines are separated by 0.1 Å or less, the mean wavelength is marked with an asterisk as in Paper I. As stated there, the best lines to use for wavelength calibration are the single lines marked with an e or an f in the figures. The next best are the blends with separation less than 0.1 Å, marked with an asterisk. Their mean wavelengths could be very slightly in error, if their e and f components differ greatly in intensity, as discussed in more detail in Sec. 4. The least desirable lines to use are blends with separations between 0.1 and 0.2 Å; they are not marked with either an asterisk or e or f on the figures. Since their separations are larger, the errors in their mean wavelengths could be proportionately larger.

In their Table 29, Abrams et al. list wavelengths of $P(J)$ and $Q(J)$ lines with $J \leq 4.5$, and of $R(J)$ with $J \leq 3.5$. For the many lines of higher J which we have identified in the OH night-sky spectrum, we have calculated the wavelengths using the energy levels deduced from their laboratory data by Abrams et al. (1994) and published in their Table 27. For the conversion from vacuum to air wavelengths we used the dispersion formula for standard air of Edlén (1953), the same one used by Abrams et al. These wavelengths are on exactly the same system as those published in their paper, and differ at most by 0.0001 Å from the air wavelengths calculated with the later dispersion formula of Edlén (1966). The lines of high J are especially useful for wavelength calibration, because their large Λ-type doubling clearly resolves the e and f components.

For completeness, these calculated wavelengths for the higher-J lines clearly observed in the night-sky spectrum in the interval 9000 Å $\leq \lambda \leq$ 10,500 Å are listed in Table 2. They are entered in the figures in the same way as the lines listed by Abrams et al. for lower J. The calculated wavelengths for the higher rotational lines with $\lambda \leq$ 9000 Å were previously published in Table 2 of Paper I.

4. DOUBLET INTENSITY RATIOS

As stated in Paper I, the intensities of the two components of each OH line, split by Λ-type doubling, are expected to be equal under the simplifying assumption of thermodynamic equilibrium. For this reason, the straight mean wavelength of all pairs which are not resolved has been adopted in this paper and in Paper I. To test this assumption we have measured the relative intensities of all the resolved pairs which have good signal-to-noise-ratio (S/N>50) in our summed spectra of Paper I and this paper. The results, in the form of intensity ratios I_e/I_f, are presented in Table 3. For these relatively strong lines the major source of error in the measured ratios seems to be the noise in the "continuum," which is probably a mixture of scattered moonlight, zodiacal light, background stars, and galaxies. All these sources have absorption lines in their spectra, which simulate noise; no doubt much of it could be considerably reduced if sufficient observing time were available. We have estimated the probable error σ in each measured intensity ratio by sketching in alternate straight lines which could conceivably be used to represent the continuum, and reducing the measurements made with them as well. The resulting probable errors are listed in the last column in Table 3. Typically, the lines with S/N $\geq$ 60 have $\sigma \leq$ 0.02, and those with S/N $\geq$ 30 have $\sigma \leq$0.03.

It can be seen that 21 of the measured intensity ratios differ from the expected value 1.00 by more than the prob-

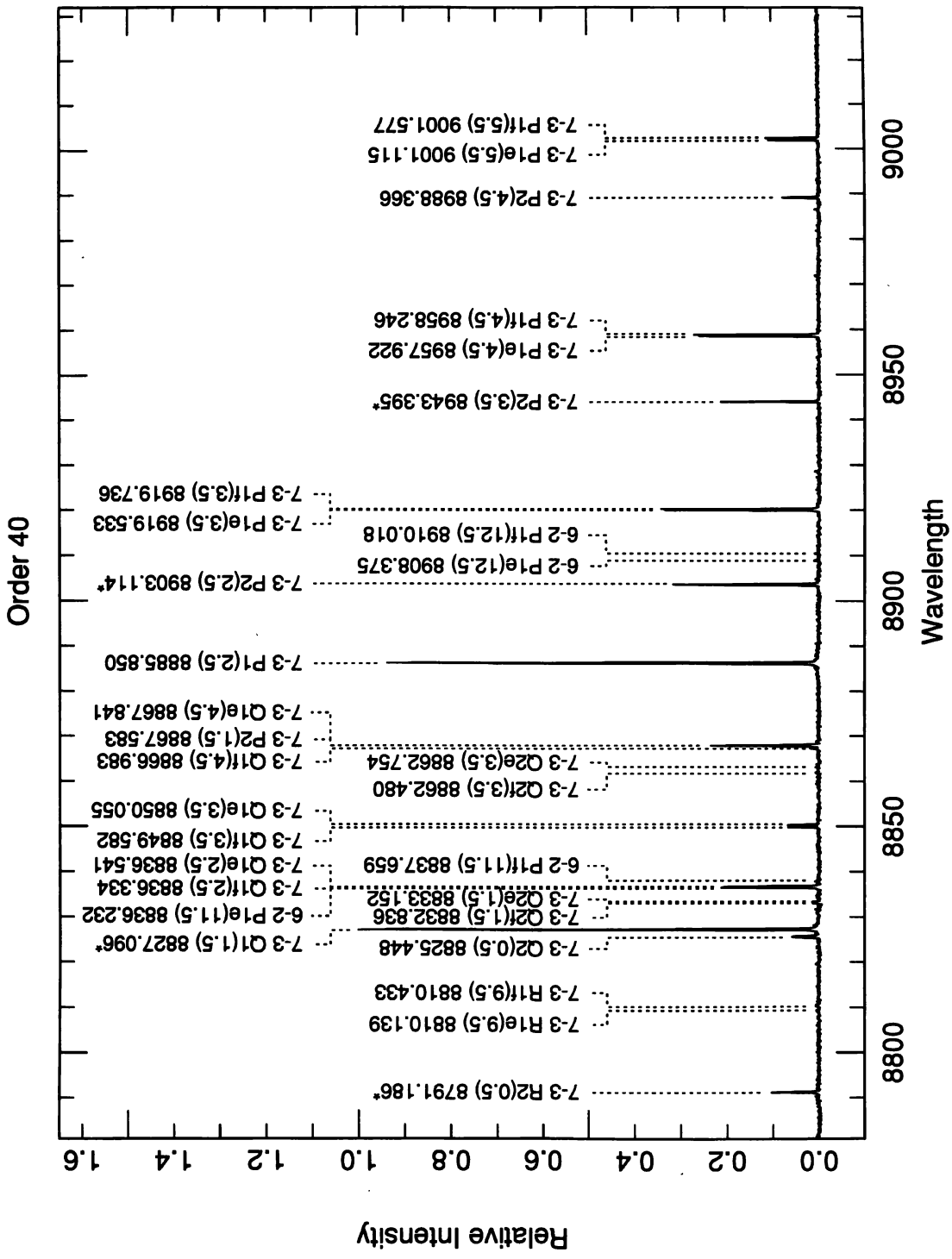

FIG. 1—Order 40 of Mauna Kea night-sky emission-line spectrum.

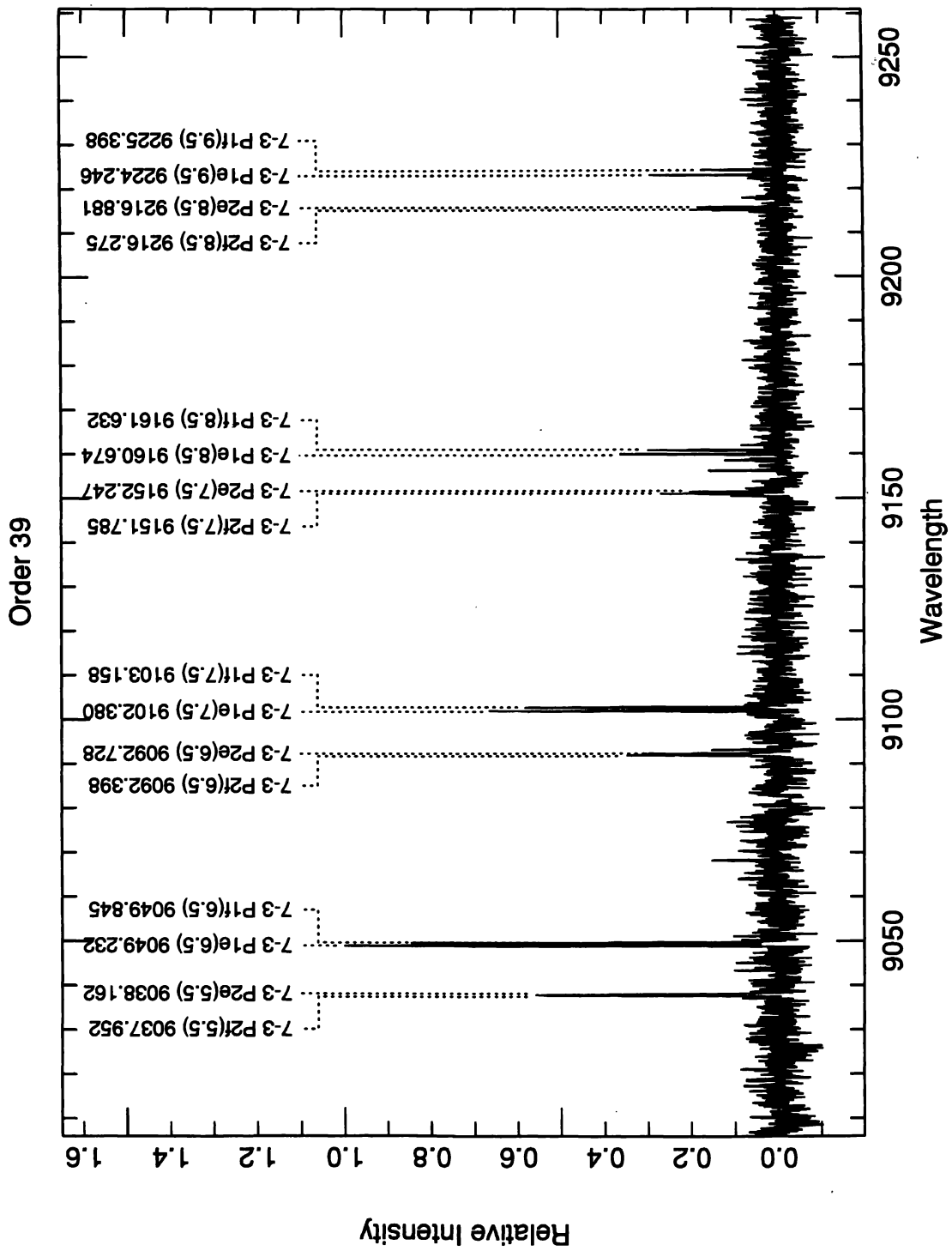

FIG. 2—Order 39 of Mauna Kea night-sky emission-line spectrum.

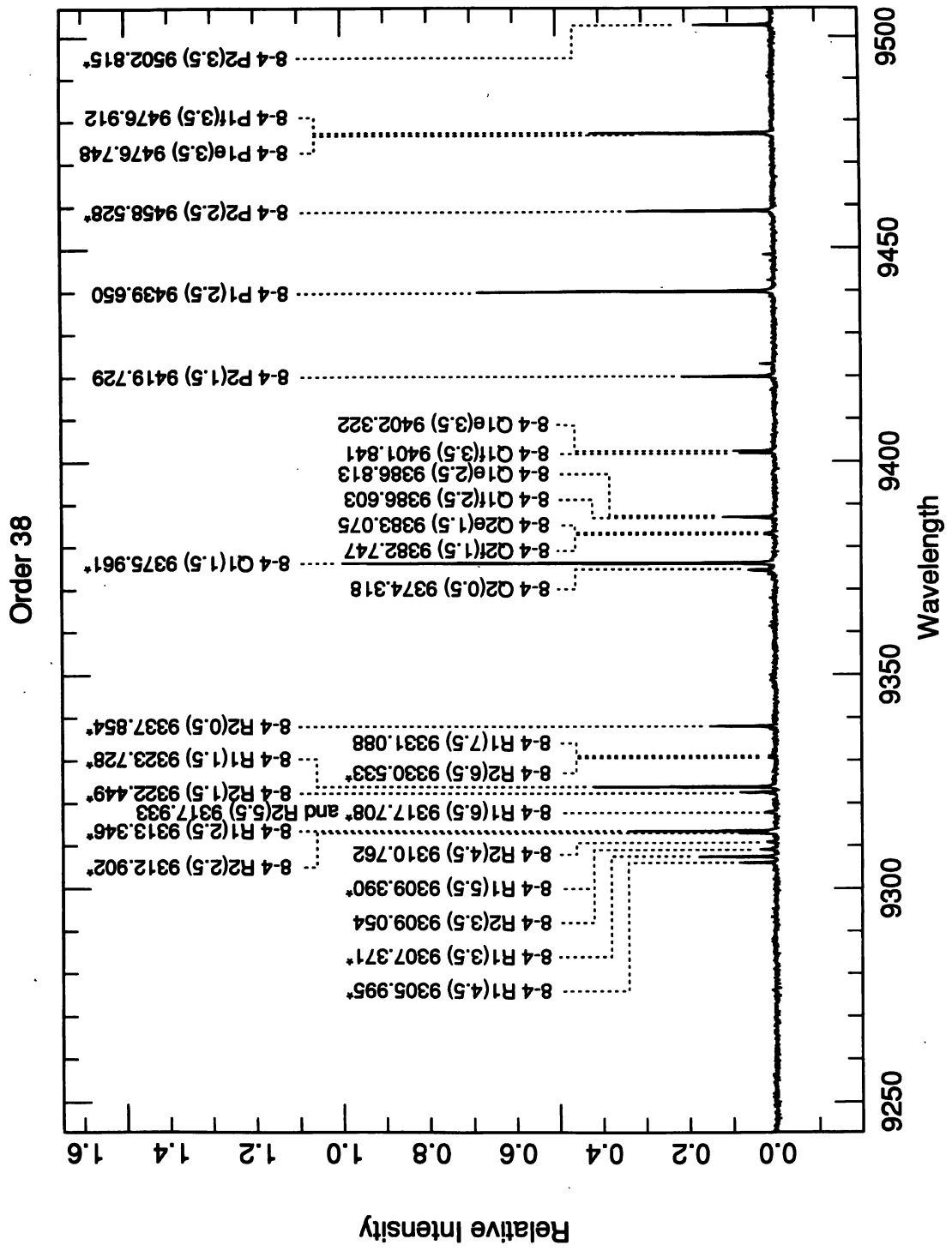

FIG. 3—Order 38 of Mauna Kea night-sky emission-line spectrum.

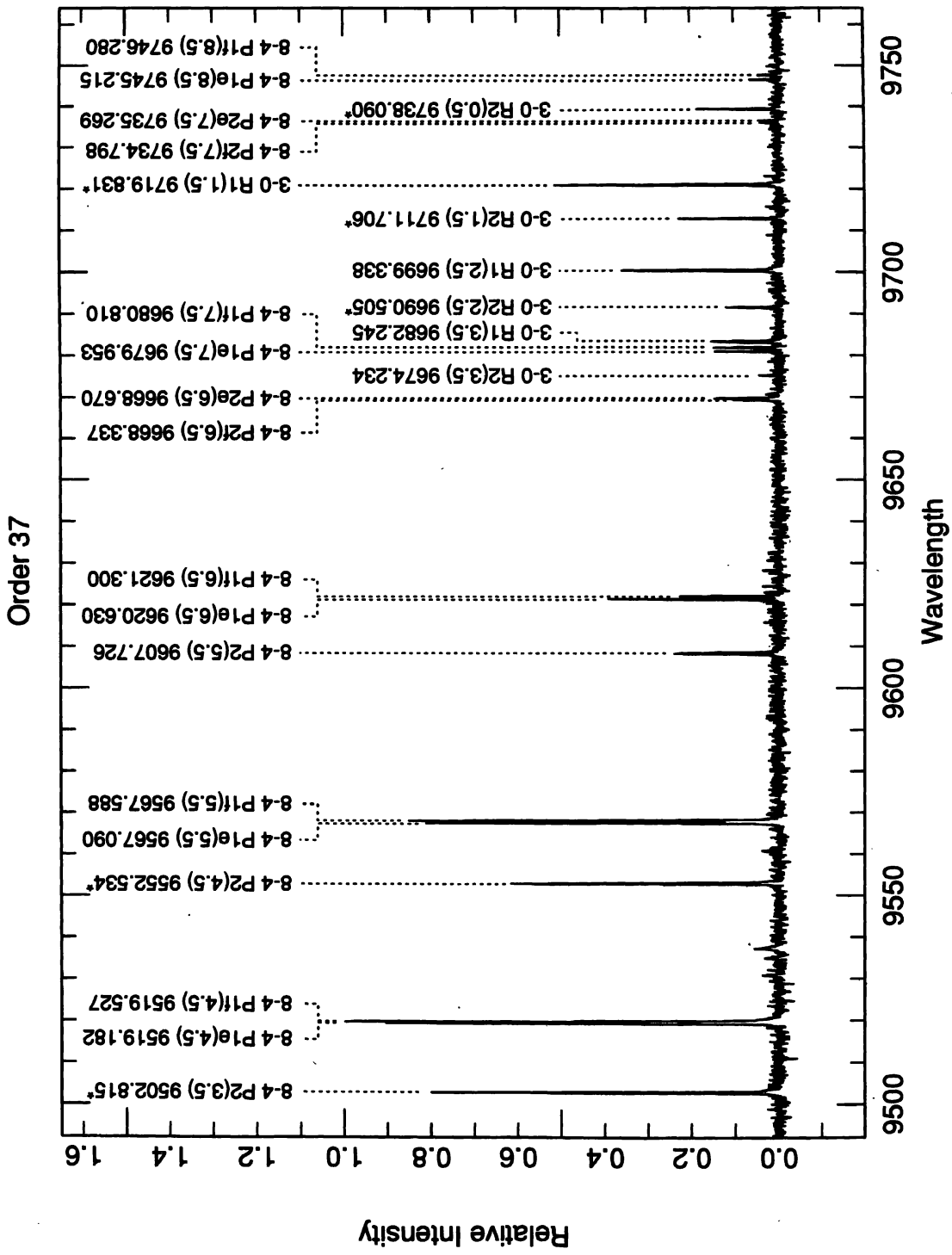

FIG. 4—Order 37 of Mauna Kea night-sky emission-line spectrum.

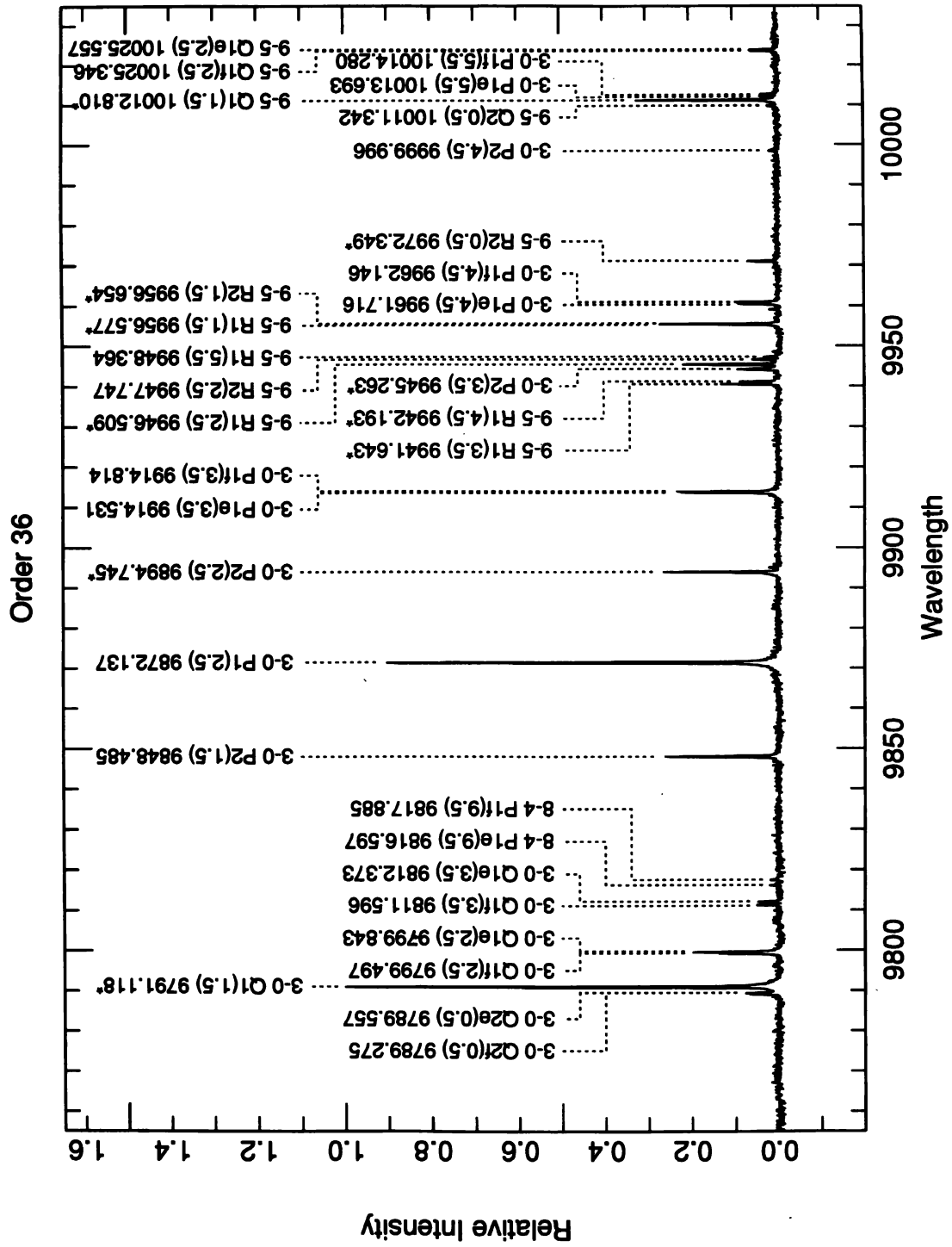

FIG. 5—Order 36 of Mauna Kea night-sky emission-line spectrum.

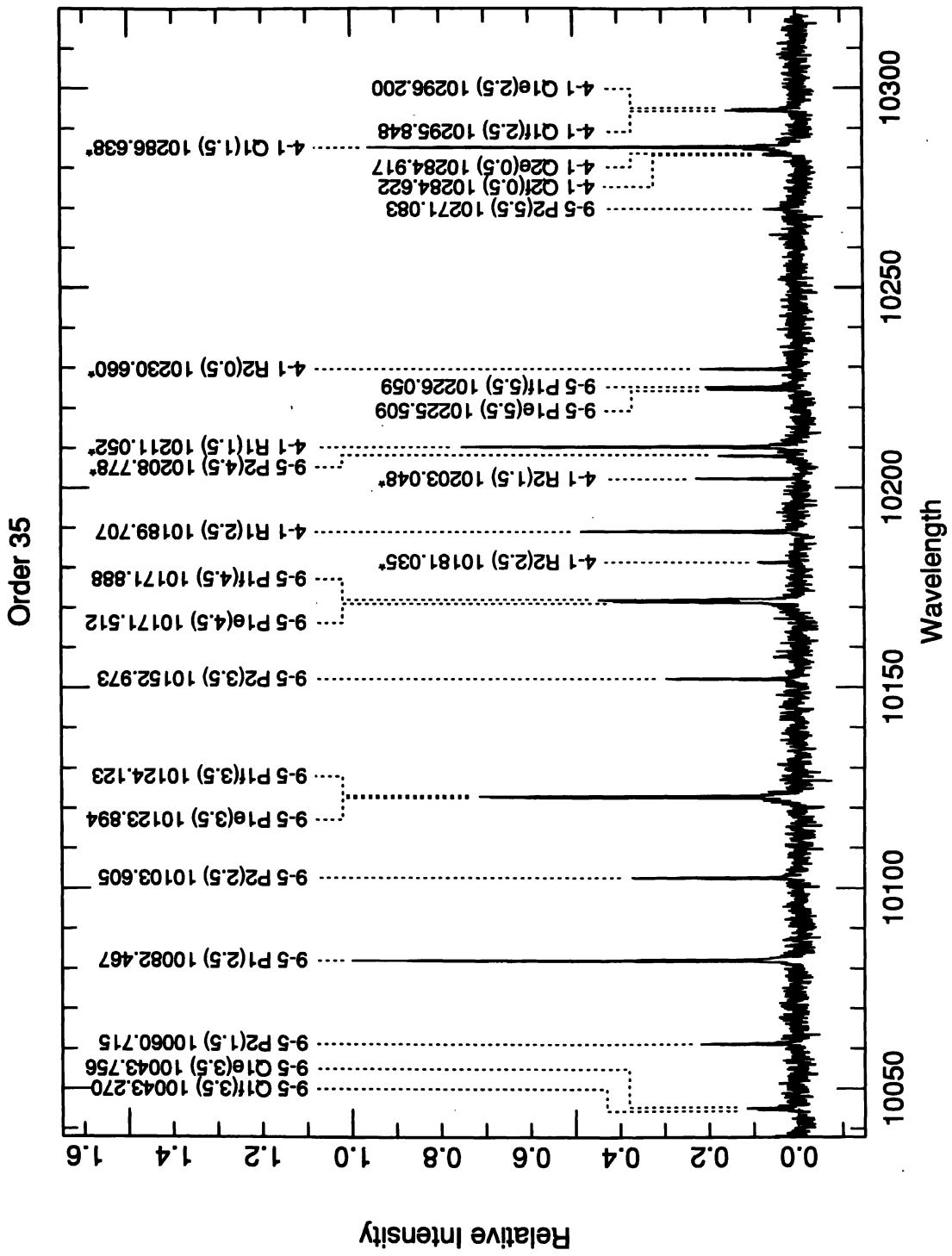

FIG. 6—Order 35 of Mauna Kea night-sky emission-line spectrum.

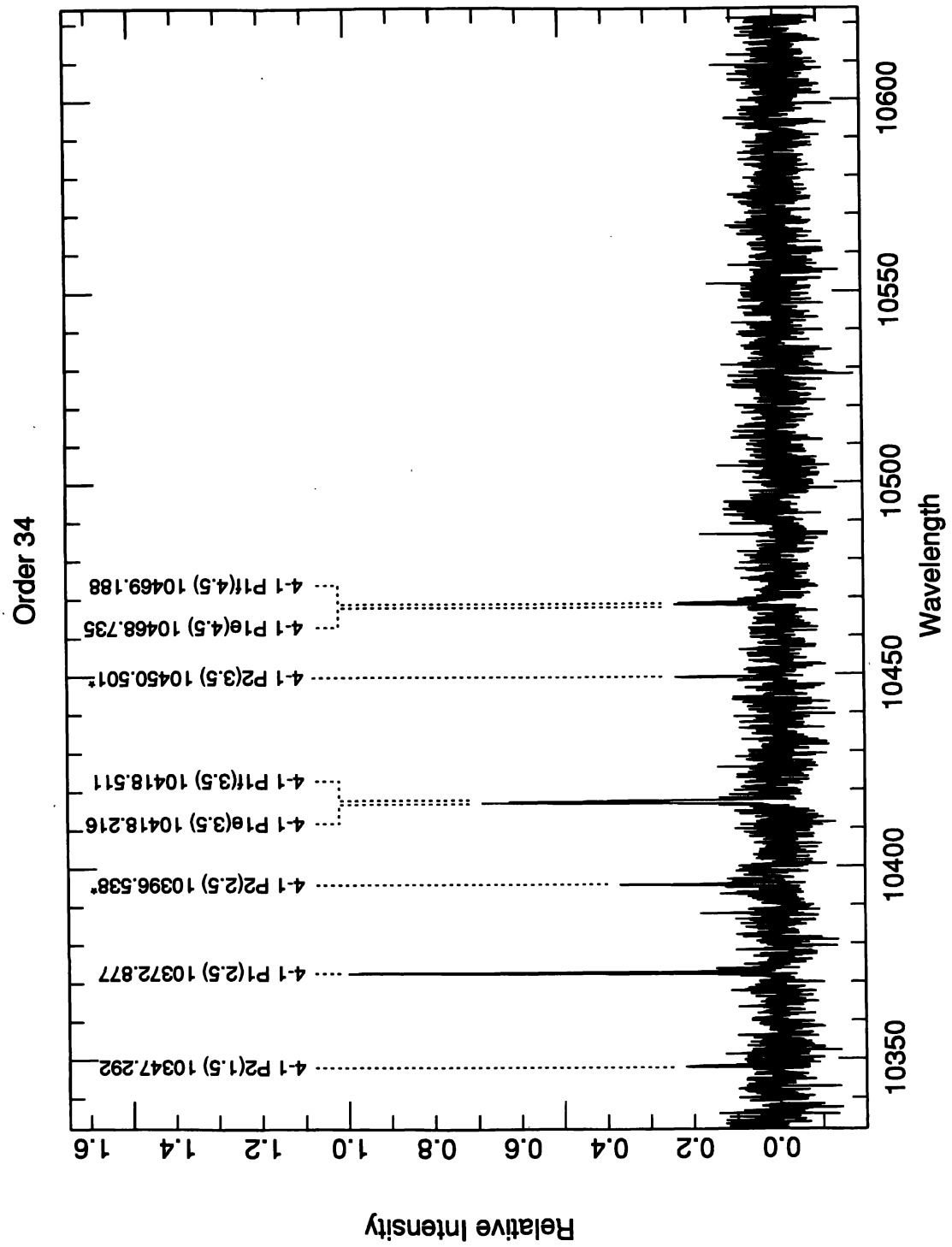

FIG. 7—Order 34 of Mauna Kea night-sky emission-line spectrum.

TABLE 2
Observed OH Lines Not Listed in Abrams et al. (1994)

v'-v"	Identificaion	Wavelength	v'-v"	Identificaion	Wavelength
7-3	P1e(5.5)	9001.115	8-4	R1e(7.5)	9330.999
7-3	P1f(5.5)	9001.577	8-4	R1f(7.5)	9331.178
7-3	P2f(5.5)	9037.952	8-4	P1e(5.5)	9567.090
7-3	P2e(5.5)	9038.162	8-4	P1f(5.5)	9567.588
7-3	P1e(6.5)	9049.232	8-4	P2f(5.5)	9607.625
7-3	P1f(6.5)	9049.845	8-4	P2e(5.5)	9607.828
7-3	P2f(6.5)	9092.398	8-4	P1e(6.5)	9620.630
7-3	P2e(6.5)	9092.728	8-4	P1f(6.5)	9621.300
7-3	P1e(7.5)	9102.380	8-4	P2f(6.5)	9668.337
7-3	P1f(7.5)	9103.158	8-4	P2e(6.5)	9668.670
7-3	P2f(7.5)	9151.785	8-4	P1e(7.5)	9679.953
7-3	P2e(7.5)	9152.247	8-4	P1f(7.5)	9680.810
7-3	P1e(8.5)	9160.674	3-0	P2f(7.5)	9734.798
7-3	P1f(8.5)	9161.632	3-0	P2e(7.5)	9735.269
7-3	P2f(8.5)	9216.275	3-0	P1e(8.5)	7945.215
7-3	P2e(8.5)	9216.881	3-0	P1f(8.5)	9746.280
7-3	P1e(9.5)	9224.246	8-4	P1e(9.5)	9816.597
7-3	P1f(9.5)	9225.398	8-4	P1f(9.5)	9817.885
8-4	R1f(4.5)	9305.982	9-5	R1e(4.5)	9942.189
8-4	R1e(4.5)	9306.009	9-5	R1f(4.5)	9942.197
8-4	R2e(4.5)	9310.701	9-5	R1e(5.5)	9948.327
8-4	R2f(4.5)	9310.822	9-5	R1f(5.5)	9948.402
8-4	R1e(6.5)	9317.663	3-0	P1e(5.5)	10013.693
8-4	R1f(6.5)	9317.753	3-0	P1f(5.5)	10014.280
8-4	R2e(5.5)	9317.878	9-5	P1e(5.5)	10225.509
8-4	R2f(5.5)	9317.988	9-5	P1f(5.5)	10226.059
8-4	R2e(6.5)	9330.493	9-5	P2f(5.5)	10270.990
8-4	R2f(6.5)	9330.574	9-5	P2e(5.5)	10271.175

able error, while eight differ from it by less than the probable error. Thus it appears that there are real deviations from the expected value 1.00 for some of these line ratios. Presumably they occur through whatever mechanisms populate the individual e and f levels of OH; if the downward radiative transition probabilities are truly independent of this symmetry property, as expected on very general principles, the difference must occur in the original formation process of the OH molecules, believed to be a two-body reaction involving O_3 and atomic H. This possibility has been discussed in some detail by Dodd et al. (1994). In no case have we been able to measure accurately an I_e/I_f ratio for a $P_1(J'')$ and a $Q_1(J'')$ with the same upper level J', which would distinguish between the population and the downward radiative transition probability as the cause of the deviation of the intensity ratio from unity. The problem is that the intensities of the $Q_1(J)$ lines decrease rapidly with increasing J, while the $P_1(J)$ splitting is too small to resolve the individual components at small J. Much longer exposure times could solve this problem.

A conceivable source of error in the measured I_e/I_f could be partial absorption of OH emission lines by atmospheric H_2O or O_2 (Espy and Hammond 1995). Given the thermal Doppler widths of the OH emission lines with T = 200–300 K, 0.02 Å as measured by Greet et al. (1994), and the somewhat broader H_2O (0.06 Å) and O_2 (0.04 Å) lines, as estimated from a high-resolution solar atlas (Delbouille et al. 1973), this would require coincidence of the emission and absorption lines to 0.05 Å or less. Of the 58 OH lines measured and listed in Table 3, none is closer than 0.04 Å to an atmospheric absorption line listed in the solar spectrum by Moore et al. (1966). In fact, the two OH emission lines closest to telluric absorption lines are (8-3) $P_{1e}(4.5)\lambda 7369.248$, which is 0.04 Å from atmospheric $H_2O\lambda 7369.206$, and (4-0) $P_{1e}(5.5)\lambda 7662.175$, which is 0.05 Å from the atmospheric O_2 line $\lambda 7662.12$. In both cases the potentially partly absorbed P_{1e} component was measured to be stronger, not weaker, than the corresponding P_{1f} component. There are only two other measured OH lines in Table 3 closer than 0.10 Å to a listed atmospheric absorption line, and only six more closer than 0.20 Å. Most of them are H_2O lines, and the great majority are very weak or do not show at all in the solar spectral atlas, observed at the Jungfraujoch at 3576 m altitude, while Mauna Kea, at 4215 m, is even higher and drier. Thus this potential alternate interpretation of deviation of the measured I_e/I_f intensity ratios from 1.00 seems to be untenable.

Whatever the source of the deviation of I_e/I_f from 1.00, it affects the measured wavelengths of the blended lines made up of the two components. If it is correct to assume that the measured wavelength of the blend is the intensity-weighted average of the wavelengths of the two components, then